ACS Catalysis

pubs.acs.org/acscatalysis
Research Article

Ultrasmall PtCo Intermetallic Compounds Confined in Silicalite-1 for Highly Productive Propane Dehydrogenation

Qiyang Zhang, Mingbin Gao, Vita A. Kondratenko, Tatiana Otroshchenko,* Xiangnong Ding, Dmitry E. Doronkin, Dongxu Wang, Dong Li, Dan Zhao,* and Evgenii V. Kondratenko*

Cite This: https://doi.org/10.1021/acscatal.5c08288

ABSTRACT: Non-oxidative propane dehydrogenation (PDH) to propene is the basis of several technologies developed for meeting the increasing demand for this olefin. Given the high cost of commercial Pt-based catalysts, a promising direction for improving the economics of propene production by PDH is to reduce Pt content without sacrificing high propene productivity and selectivity. We report that the 1Co-0.1Pt@silicalite-1(1Co-0.1Pt@S-1) catalyst, with only 0.1 wt% Pt and 1 wt% Co, outperforms an analog of commercial Pt–Sn/Al_2O_3 in terms of activity and on-stream stability despite the approximately 5-fold lower Pt loading. Its performance is also remarkable when compared to other state-of-the-art Pt-containing catalysts. The high activity of the 1Co-0.1Pt@S-1 catalyst is attributed to the presence of ultrasmall PtCo intermetallic compounds formed under reaction conditions. The developed catalyst also demonstrated high on-stream stability, with an apparent deactivation rate constant of just 4×10^{-4} h^{-1} determined over 110 h on stream at approximately 90% of the equilibrium propane conversion at 500 °C using a feed with 90 vol % propane.

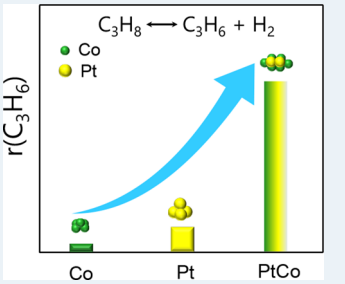

KEYWORDS: *propane dehydrogenation, PtCo intermetallic compounds, in situ XAS, silcalite-1, propene production*

INTRODUCTION

Propene is a key petrochemical used in the manufacture of various products.[1−3] Current large-scale technologies for its production are steam or fluid catalytic cracking of different crude oil fractions,[4] methanol-to-olefins conversion,[5] metathesis of ethene with 2-butene,[6] Fisher–Tropsch synthesis to olefins,[7] and non-oxidative propane dehydrogenation (PDH).[8] The latter technology has attracted extensive attention due to the shale gas revolution.[9] Supported Pt-containing catalysts have been widely used for the PDH reaction due to their ability to activate selectively the C–H bonds but not to cleave the C–C bonds in propane, ensuring high propene selectivity.[10,11] However, there are still challenges related to their activity, durability, and, especially, cost.

An efficient method to improve catalyst activity and propene selectivity is the use of supported Pt intermetallic compounds with Sn,[12−14] Ge[15], Ga,[16] Zn,[17] In,[18] or Cu.[19,20] The promoters increase the electron density of Pt and thus weaken Pt–propene binding, thereby inhibiting deep dehydrogenation reactions leading to coke.[21] The potential of bimetallic Co–Pt catalysts has only occasionally been tested, although Co-containing catalysts show attractive performance.[22,23] For example, Miller and coworkers[21] found Co as an efficient promoter for Pt/SiO_2 catalysts due to the dilution of large surface Pt ensembles. The Pt_3Co surface structure of the PtCo species was concluded to be responsible for propene production. However, such catalysts have been tested using a feed with only 2 vol % propane, which is unfavorable from an application point of view. Very recently, Xin-Hao Li and coworkers developed Co–Pt-based catalysts using a nitrogen-doped carbon support.[24] In contrast to Miller and coworkers,[21] separated Co and Pt centers are needed for efficient propane dehydrogenation to propene. The best-performing catalyst deactivated slowly and showed about 90% propene selectivity, but in the presence of co-fed hydrogen. The selectivity decreased without co-fed hydrogen strongly. In addition, the impact of the developed catalysts was not demonstrated by comparison with state-of-the-art catalysts. It should also be noted that all PtCo-based catalysts developed to date have a relatively high Pt content (>0.5 wt%), which is detrimental for large-scale applications.

Motivated by the above challenges, herein we elucidate the fundamentals of the effect of minute amounts of Pt on PDH performance of Co-based catalysts. Siliceous zeolites, with ordered pore structures, high hydroxyl defect density, and excellent thermal stability, are more suitable for anchoring ultrasmall metal clusters compared to amorphous SiO_2 supports. In the present study, microporous silicalite-1 zeolite (S-1) was selected as a support to confine small monometallic or bimetallic species within its channels during hydrothermal crystallization by a ligand-protected approach (Table S1).

Received: November 19, 2025
Revised: April 7, 2026
Accepted: April 13, 2026

https://doi.org/10.1021/acscatal.5c08288
ACS Catal. XXXX, XXX, XXX−XXX

The best-performing 1Co-0.1Pt@S-1 catalyst with 0.1 wt% of Pt and 1 wt% of Co showed unexpectedly high space–time yield of propene formation, on-stream stability, and durability. Its outstanding performance was explained by the presence of ultrasmall PtCo intermetallic compounds with an atomic ratio of Pt:Co of 1:3 (Figure S1), which are different from those in ref 21, as concluded by aberration-corrected scanning transmission electron microscopy (AC-STEM) and in situ X-ray absorption spectroscopy (XAS) analysis. Temporal analysis of products revealed the fundamentals of the synergistic effect between Pt and Co in terms of H_2 activation. This catalyst property is highly relevant for enhancing the turnover frequency through the formation of H_2 in the course of the PDH reaction. The knowledge gained is relevant for the targeted design of catalysts not only for this reaction but also for hydrogenation reactions and paves the way toward the development of highly active low-loaded Pt-containing catalysts.

EXPERIMENTAL PART

Catalyst Preparation

The following chemicals were used as received: tetraethylorthosilicate (25 wt % TEOS, Sigma-Aldrich), $Co(NO_3)_2{\cdot}6H_2O$ (99%, Sigma-Aldrich), tetrapropylammonium hydroxide (TPAOH, Sigma-Aldrich), ethylenediamine (EDA, 99%, Merck), $[Pt(NH_3)_4](NO_3)_2$ (≥50.0% Pt basis, Sigma-Aldrich), H_2PtCl_6 solution (8 wt % H_2PtCl_6, Merck), $SnCl_2{\cdot}2H_2O$ (99.99%, Sigma-Aldrich), ethanol (99.9%, Thermo Fisher), and commercial γ-Al_2O_3 (>99.9%, Saint-Gobain, 93 $m^2{\cdot}g^{-1}$).

1Co@S-1 was synthesized via a modified hydrothermal synthesis method. 0.0998 g of $Co(NO_3)_2{\cdot}6H_2O$ was dissolved in 8 mL of EDA to prepare a Co-EDA precursor solution. In a separate step, 11.2 g of TPAOH was added to 14.7 mL of deionized water and stirred for 10 min. Subsequently, 7.2 g of TEOS was added to the TPAOH solution under continuous stirring for 6 h. Then, the Co-EDA precursor solution was added to the TEOS-TPAOH solution. After further stirring for 2 h, the obtained clear solution was transferred into a 70 mL Teflon-lined stainless-steel autoclave and crystallized in a conventional oven at 170 °C for 4 days under a static condition. The solid product was collected after washing, centrifugation, and drying at 100 °C overnight. Thereafter, it was finally calcined at 550 °C for 6 h to obtain 1Co@S-1.

1Co-0.1Pt@S-1 was synthesized using a similar method to that described above. 0.0998 g of $Co(NO_3)_2{\cdot}6H_2O$ and 0.0040 g of $Pt(NH_3)_4](NO_3)_2$ were dissolved in 8 mL of EDA to prepare a CoPt-EDA precursor solution. The synthesis of 1Co-xPt@S-1 was carried out using a method similar to that described above for the preparation of the 1Co@S-1 catalyst. The metal mass ratios of Co/Pt were set to 100/1, 20/1, 10/1, and 5/1 to obtain the 1Co-0.01Pt@S-1, 1Co-0.05Pt@S-1, 1Co-0.1Pt@S-1, and 1Co-0.2Pt@S-1 catalysts, respectively.

The M@S-1 series samples (0.01Pt@S-1, 0.05Pt@S-1, 0.1Pt@S-1, and 0.2Pt@S-1) were also synthesized via a similar method as described for 1Co-M@S-1 but without adding the cobalt precursor.

An analog of industrial Pt–Sn/Al_2O_3 (containing 0.5 wt % Pt and 1.5 wt % Sn) was prepared by impregnation according to ref 25. First, a solution containing metal precursors was prepared by dissolving 0.628 g of H_2PtCl_6 (8 wt%H_2Cl_6Pt; Aldrich) and 0.145 g of $SnCl_2{\cdot}2H_2O$ (99.99%, Sigma-Aldrich) in 30 ml of ethanol (99.9%, Thermo Fisher). Thereafter, 5 g of a commercial Al_2O_3 carrier (Saint-Gobain, 93 $m^2{\cdot}g^{-1}$) was impregnated with the solution. The obtained sample was dried in an an oven at 100 °C for 12 h and then calcined at 560 °C for 3 h in air.

Catalyst Characterization

X-ray diffraction (XRD) patterns of the as-prepared catalysts were recorded on a Bruker D8 Advance operating at 40 kV and 100 mA. Cu Kα radiation (0.15406 nm) was used.

Ex situ UV–vis spectra were recorded between 200 and 1200 nm on a Shimadzu UV-2600 with $BaSO_4$ as a white standard.

High-resolution transmission electron microscopy (HRTEM) was conducted on an FEI Talos 200X with a working voltage of 200 kV, and the aberration-corrected high-angle angular dark-field-scanning transmission electron microscopy (AC-HAADF-STEM) was conducted on a JEM-ARM300F operated at 300 kV to identify the microstructure and elemental distribution of the prepared catalysts.

X-ray photoelectron (XP) spectroscopy was applied for catalyst surface characterization using an ESCALAB 220iXL (Thermo Fisher Scientific) setup with monochromatic Al Kα radiation (E =1486.6 eV). The samples were prepared on a stainless-steel holder with conductive double-sided adhesive carbon tape. The electron binding energies were obtained with charge compensation using a flood electron source and referenced to the C 1s core level of adventitious carbon at 284.8 eV (C–C and C–H bonds).

Before starting C_3H_8-TPSR tests, all catalysts (25 mg for each sample) were calcined at 500 °C in flowing air for 1 h and then reduced in a flow (5 vol % H_2 in Ar, total flow of 10 $mL{\cdot}min^{-1}$) for 60 min. After the above treatment, the reactors with the treated catalysts were cooled down to 200 °C. Thereafter, the reactors were flushed with Ar for 30 min and exposed to a flow of C_3H_8/Ar = 10/90 (10 $mL{\cdot}min^{-1}$). The temperature was initially kept at 200 °C for 15 min to stabilize mass spectroscopic signals. Then, the catalysts were heated up to 450 °C with a heating rate of 10 $K{\cdot}min^{-1}$. The signals at m/z of 44 (C_3H_8), 42(C_3H_6), 2 (H_2), and 40 (Ar) were collected. The contribution of propane to the propene signal was separately determined using a calibration mixture with 10 vol % C_3H_8 in Ar and subtracted from the overall signal at m/z of 42.

X-ray absorption spectra (XANES and EXAFS) at the Co K and Pt L3 absorption edges were recorded at the P65 beamline of the PETRA III synchrotron radiation source (DESY, Hamburg) in fluorescence mode. Higher harmonics were rejected by a pair of Si plane mirrors installed in front of the monochromator. The energy of the X-ray photons was further selected by a Si (111) double-crystal monochromator, and the beam size was set by means of slits to 0.4 (vertical) × 2.0 (horizontal) mm^2. Pt L_3-edge spectra were recorded using a large-area 4-element silicon drift detector (2 mm thick Hitachi Vortex-ME4) coupled with an XGLab DANTE digital pulse processor. Spectra were recorded in continuous mode while scanning incident energy from −150 to +800 eV relative to the respective absorption edge, with a total time of 180 and 0.1 s per point integration time. The spectra were normalized, and the extended X-ray absorption fine structure spectra (EXAFS) background was subtracted using the ATHENA program from the IFEFFIT software package.[26] The k^2-weighted EXAFS functions were Fourier transformed (FT) in the k range of 2–10 $Å^{-1}$ and multiplied by a Hanning window with a sill size of 1 $Å^{-1}$. The displayed FT EXAFS spectra were not corrected for the phase shift. For in situ XANES, the measured sample with a sieve fraction of 100–200 μm was loaded in an in situ micro-reactor (quartz capillary, 1.5 mm diameter, 0.02 mm wall thickness). The sample was heated stepwise to 500 °C with a ramp of 10 °C/min under He (20 $mL{\cdot}min^{-1}$ flow rate). After reaching the temperature, the sample was calcined in a flow of 20 vol % O_2 in He (20 $mL{\cdot}min^{-1}$) for 30 min and then reduced in a flow of 50 vol % H_2 in He (20 $mL{\cdot}min^{-1}$ flow rate) for 30 min. The in situ spectra were recorded during the whole experiment. To increase the signal-to-noise ratio, Pt L_3 spectra recorded under the respective steady-state conditions were monitored for changes in the XANES region (which stopped changing within 10 min after reaching steady-state conditions) and averaged together for further analysis.

Temporal Analysis of Products

The mechanistic and kinetic aspects of propane dehydrogenation were examined using a temporal analysis of products (TAP-2) reactor. The reactor system, operating with millisecond resolution, has been described in detail elsewhere.[27] In these experiments, 30 mg of

https://doi.org/10.1021/acscatal.5c08288
ACS Catal. XXXX, XXX, XXX–XXX

1Co@S-1, 0.1Pt@S-1, or 1Co-0.1Pt@S-1 (315–710 μm fraction) was loaded in a quartz-tube reactor and fixed within its isothermal zone between two layers of quartz particles of 250–355 μm size. Prior to the experiments, the catalysts were heated from room temperature to 500 °C in a flow of N_2 (3 mL·min^{-1}) and H_2 (2 mL·min^{-1}). Then, the catalysts were held in the same flow at this temperature for 1 h. After finishing the treatment, the reactor with the catalyst was evacuated to ca. 10^{-5} Pa, and the pulse experiments with C_3H_8:Ar = 1:1 or D_2:Ar = 1:1 mixtures were carried out at 500 °C. The mixtures were prepared using C_3H_8 (Linde, 3.5), D_2 (Aldrich, 99.8 atom. % D), and Ar (Air Liquide, 5.0) without additional purification.

The composition of the gas mixture at the reactor outlet was monitored by a quadrupole mass spectrometer (HAL RC 301 Hiden Analytical). The following m/z values were used for mass spectrometric identification of different compounds: 44 (C_3H_8), 42 (C_3H_8, C_3H_6), 41 (C_3H_8, C_3H_6), 29 (C_3H_8), 28 (C_3H_8, C_2H_6, C_2H_4), 26 (C_3H_8, C_3H_6, C_2H_6, C_2H_4), 16 (CH_4), 4 (D_2), 3 (HD), 2 (H_2), and 40 (Ar). The pulses for each m/z were repeated 10 times and averaged to improve the signal-to-noise ratio. The contribution of different compounds to respective m/z was estimated using standard fragmentation patterns determined in separate experiments.

For proper analysis of the relative positions of the transient responses of reaction components strongly differing in their diffusivity (C_3H_8 vs. H_2 or D_2 vs. H_2), the experimental time (t) of respective responses was converted into dimensionless form as suggested in ref 27 according to eq 1.

$$\tau = \frac{t\, D_{\mathrm{eff,i}}}{\varepsilon_b L^2} \tag{1}$$

where ε_b is the fractional voidage of the packed bed in the reactor, L is the diffusion length (m), and $D_{\mathrm{eff,i}}$ is the effective diffusion coefficient of each component (m^2/s). The whole reactor length was considered as a diffusion length for reactants, whereas for the reaction products, the diffusion length was set from the beginning of the catalyst layer.

The apparent rate constant $k_{D_2}^{\mathrm{app}}$ for D_2 consumption was determined as suggested in ref 28 (eq 2).

$$k_{D_2}^{\mathrm{app}} = \frac{X}{\varepsilon_b \frac{\Delta L \cdot L_{II}}{D_{\mathrm{eff},D_2}} (1 - X)} \tag{2}$$

where ε_b is the fractional voidage of the packed bed in the reactor, X is D_2 conversion, D_{eff,D_2} is the effective diffusion coefficient of D_2 (m^2/s), ΔL is the thickness of the catalyst layer (m), and L_{II} is the thickness of the downstream inert layer (m). The effective diffusion coefficients were calculated from that of Ar (eq 3). The effective diffusion coefficient of Ar was determined separately from the fitting of the Ar experimental response to the model assuming diffusion only, according to the procedure described in ref 29. M_{Ar} is the molecular weight of Ar. M_i is the molecular weight of gas i.

$$D_{\mathrm{eff,i}} = D_{\mathrm{eff,Ar}} \sqrt{\frac{M_{\mathrm{Ar}}}{M_i}} \tag{3}$$

Catalytic Tests

All catalytic tests were carried out at 500, 525, and 550 °C under 1 bar in an in-house developed setup consisting of 15 continuous-flow fixed-bed quartz reactors. The rate of propene formation was determined at a degree of propane conversion below 10% after the first 240 s on propane stream. Typically, the catalysts (10 mg, fraction of 315–710 μm) were heated to 500 °C in a N_2 flow with a heating rate of 10 K·min^{-1}. After reaching the reaction temperature, the sample was treated in a flow of 20 vol % O_2 in N_2 (20 mL·min^{-1}) for 30 min, followed by feeding N_2 for 10 min to remove oxygen from the reactor. Thereafter, a flow of 50 vol % H_2 in N_2 (20 mL·min^{-1} flow rate) was fed for 30 min. After the treatment, the catalysts were tested with a reaction mixture of 40 vol % C_3H_8 in N_2.

A durability test using the 1Co-0.1Pt@S-1 catalyst consisted of a series of six PDH/regeneration cycles at 500 °C using a feed with 40 vol % C_3H_8 in N_2 at a WHSV of 94.3 h^{-1}. The catalyst was calcined in 20 vol % O_2/N_2 (10 mL·min^{-1}) for 15 min after each PDH cycle and then reduced in 50 vol % H_2/N_2 (10 mL·min^{-1}) for 60 min at 500 °C before starting PDH. The catalyst was purged with N_2 (10 mL·min^{-1}) for 15 min between each step.

To determine the apparent activation energy of propene formation, catalytic tests were carried out in the temperature range of 465–545 °C at propane conversion below 10%. To this end, the catalyst amount and the total feed flow were varied from 10 to 100 mg and from 10 to 80 mL·min^{-1}, respectively.

$$r(C_3H_6) = \frac{\dot{n}(C_3H_6)}{V_m \times m_{\mathrm{cat}}} \tag{4}$$

where $\dot{n}(C_3H_6)$ is the molar flow of propene. V_m and m_{cat} stand for the molar volume (22.4 mL·mmol^{-1}) and catalyst mass, respectively.

To compare the different catalysts (1Co-0.1Pt@S-1 and PtSn/Al_2O_3) with respect to time-on-stream activity and stability, they (15 mg, fraction 315–710 μm) were initially heated to 500 °C at a rate of 10 °C·min^{-1} in a N_2 flow, followed by feeding air for 60 min and purging with N_2 for 15 min. Then, the catalysts were reduced in a flow of 50 vol % H_2 in N_2 (total flow of 10 mL·min^{-1}) for 60 min at 500 °C. The treated catalysts were directly tested for their PDH activity at 500 °C (40 vol % C_3H_8 in N_2 reaction mixture, total flow of 10 mL·min^{-1}). Propane conversion ($X(C_3H_8)$) and propene selectivity ($S(C_3H_6)$) were calculated according to eqs 5 and 6, respectively. The outlet propene concentration ($C(C_3H_6)_{\mathrm{out}}$) was calculated according to eq 7.

$$X(C_3H_8) = \frac{\dot{n}^{\mathrm{in}}_{C_3H_8} - \dot{n}^{\mathrm{out}}_{C_3H_8}}{\dot{n}^{\mathrm{in}}_{C_3H_8}} \tag{5}$$

$$S_i = \frac{\nu_{C_3H_8}}{\nu_i} \times \frac{\dot{n}^{\mathrm{out}}_i}{\dot{n}^{\mathrm{out}}_{C_3H_8} - \dot{n}^{\mathrm{out}}_{C_3H_8}} \tag{6}$$

$$C(C_3H_6)_{\mathrm{out}} = C_{C_3H_8} \times X(C_3H_8) \times S(C_3H_6) \tag{7}$$

$\dot{n}$ ($\dot{n}_i$ or $\dot{n}_i^{\mathrm{out}}$) with superscripts in or out stands for the molar flows of gas-phase components at the reactor inlet or outlet. Here, ν_i is the stoichiometric coefficient for product i. $C_{C_3H_8}$ stands for the concentration of propane in the reaction feed. N_2 was used as an internal standard to consider reaction-induced changes in the number of moles. The ratio of the molar fraction of N_2 at the reactor inlet to that at the reactor outlet was used to calculate the molar flows of gas-phase components at the reactor outlet from their outlet molar fractions and the total molar feed flow. To demonstrate long-term stability in the course of propane dehydrogenation, additional tests were performed at 500 °C. The catalysts (30 mg, fraction 315–710 μm) were heated in a N_2 flow to the reaction temperature with a rate of 10 °C·min^{-1}, followed by feeding air for 60 min and purging with N_2 for 15 min. After this treatment, the catalysts were directly tested for their PDH activity (90 vol % C_3H_8 in N_2 reaction mixture, total flow of 10 mL·min^{-1}) at 500 °C for 110 h. The long-term stability was also checked at 525 and 550 °C under the above-mentioned test conditions. The space–time yield of propene formation ($STY(C_3H_6)$) was calculated according to eq 8.

$$STY_{(C_3H_6)} = \frac{\dot{n}(C_3H_6) \times M_{(C_3H_6)} \times 60}{1000 \times m_{\mathrm{cat}}} \tag{8}$$

https://doi.org/10.1021/acscatal.5c08288
ACS Catal. XXXX, XXX, XXX–XXX

As suggested in ref 30, an apparent catalyst deactivation constant (k_d) was calculated according to eq 9.

$$k_d = \frac{\ln\frac{1-X_{end}}{X_{end}} - \ln\frac{1-X_{start}}{X_{start}}}{t} \quad (9)$$

X_{start} and X_{end} stand for propane conversion after 4 min and 110 h on stream, respectively.

An online gas chromatograph (Agilent 6890) equipped with PLOT/Q (for CO_2), AL/S (for CH_4, C_2H_4, C_2H_6, C_3H_6, and C_3H_8) columns connected to a flame ionization detector, and with a Molsieve 5 (for H_2, O_2, N_2, and CO) column connected to a thermal conductivity detector was used for quantifying the concentrations of the feed components and the reaction products. The time taken for one analysis was 5 min.

To calculate the ratio of $X(C_3H_8)_{exp}/X(C_3H_8)_{eq}$, where $X(C_3H_8)_{exp}$ and $X(C_3H_8)_{eq}$ are the experimentally determined and equilibrium conversion, respectively, we proceeded as follows. It is well known that $X(C_3H_8)_{eq}$ depends on the feed composition, reaction temperature, and total pressure. The respective data from the present and previously reported studies were used to calculate the equilibrium mole fractions ($\chi(i)_{eq}$) of propane, propene, and hydrogen using the Cantera package (https://cantera.org/) and the NASA thermodynamic database (B.J. McBride, S. Gordon, and M.A. Reno, "Coefficients for Calculating Thermodynamic and Transport Properties of Individual Species", NASA Report TM-4513, October 1993; https://shepherd.caltech.edu/EDL/PublicResources/sdt/refs/NASA-TM-4513.pdf) implemented in a Python program. Reaction-induced changes in the number of moles were considered. Based on the feed fraction of propane ($\chi(C_3H_8)_{feed}$) and the calculated equilibrium propane fraction ($\chi(C_3H_8)_{eq}$), the equilibrium conversion of propane can be calculated according to eq 10.

$$X(C_3H_8)_{eq} = \frac{\chi(C_3H_8)_{feed} - \chi(C_3H_8)_{eq}}{\chi(C_3H_8)_{feed}} \quad (10)$$

Using the $X(C_3H_8)_{exp}$ and $X(C_3H_8)_{eq}$ values determined as described above, the ratio of $X(C_3H_8)_{exp}/X(C_3H_8)_{eq}$ was calculated for each catalyst.

DFT Calculations

The structure file of the MFI framework was downloaded from the Zeolite Associations (IZA) website. Based on the catalyst characterization data, we constructed the theoretical model, Pt_4Co_{12}@S-1,of the 1Co-0.1Pt@S-1 catalyst. The energy barriers of the elementary steps in the course of the PDH reaction were estimated by spin-polarized periodic DFT calculations using the plane-wave pseudopotential method and the generalized gradient approximation (GGA). Preliminary geometry optimization of the constructed structure was implemented with the CASTEP code. The plane-wave basis set was converged at a cutoff energy of 500 eV for each model. The Perdew–Burke–Ernzerhof (PBE) exchange–correlation functional was used to describe the exchange–correlation effects. Interaction between the valence electrons and the ion core was substituted by an ultrasoft pseudopotential. The self-consistent convergence accuracy was set at 2×10^{-5} eV per atom, the maximum force was 0.08 eV per Å, the maximum stress was 0.1 GPa, and the maximum displacement was 5×10^{-3} Å. Here, a single unit cell of the MFI framework was employed. A Monkhorst–Pack grid of $1 \times 1 \times 1$ k-points was used to sample the Brillouin zone. Subsequent calculations related to the propane dehydrogenation reaction pathway were performed using the Vienna Ab initio Simulation Package (VASP). The DFT-D3 method of Grimme[31] was employed in all calculations to treat van der Waals interactions. An energy cutoff of 500 eV was applied. Geometry optimization was converged until the forces acting on the atoms were lower than 0.02 eV/Å. The energy threshold defining self-consistency of the electron density was set to 2×10^{-5} eV. The climbing image nudged elastic band method[32] and the improved dimer method[33] were applied for finding transition states. Harmonic frequencies of adsorbates and transition states were calculated, and zero-point energy (ZPE) corrections resulted from the frequency analysis were included in the calculated energies. Zero-point energies and the Gibbs free energies for the reaction temperature of 500 °C and ambient pressure were calculated using the VASPKIT program.[34] Gas-phase molecules (C_3H_8, C_3H_6, H_2) were calculated in a cubic box of 30 Å to avoid interactions between periodic images. Thermal corrections to the Gibbs free energy at 500 °C were applied based on gas-phase statistical thermodynamics, including contributions from translational, rotational, and vibrational motions. These corrections were also obtained with the help of the VASPKIT program.

RESULTS AND DISCUSSION

Results

Catalysts Characterization. X-ray diffraction (XRD) analysis revealed the MFI structure in all catalysts, with no evidence for the presence of nanocrystalline mono- or bimetallic species (Figure S2). The high dispersion of cobalt was also confirmed by UV–vis spectroscopy. The UV–vis spectra are characterized by bands at 497, 576, and 658 nm, typical for highly dispersed pseudo-tetrahedral $Co^{2+}O_x$ species (Figure S3).[22,23] The divalent cobalt in 1Co@S-1 and 1Co-0.1Pt@S-1 was determined by X-ray photoelectron spectroscopy (XPS) based on the Co $2p_{3/2}$ binding energy at about 781.7 eV (Figure S4).[35]

In situ XAS measurements provided insights into the local coordination of Co and Pt in mono- and bi-metallic catalysts. The features in the XANES spectrum of fresh 1Co@S-1 are similar to those of CoO (Figure 1a). When the catalyst was heated to 500 °C in He, the intensity of the white line decreased strongly (Figure S5), while the intensity of the pre-edge increased slightly, but its position remained unchanged (Figure 1a). As the pre-edge of the 3d elements is sensitive to both their coordination environment and symmetry,[36,37] such changes should be due to the removal of adsorbed water. The XANES spectrum did not change when He was replaced by O_2. According to the fit of the EXAFS spectrum of the fresh 1Co@S-1 catalyst, this material should possess small CoO_x clusters with coordination numbers (CNs) in the Co–O, Co–Si, and Co–O–Co shells of about 4, 1, and 4, respectively (Table S2). The intensity of the pre-edge region slightly increased after catalyst treatment in H_2 (Figure 1a). This can be attributed to a partial reduction of $Co^{2+}O_x$.[36] This assumption is supported by the decrease in the CNs in Co–O and Co–O–Co to about 3.5 and 2.4, respectively (Table S2). The fraction of metallic Co^0 in the reduced 1Co@S-1 catalyst is about 2%, as determined by O_2-pulse experiments (Figure S6a).

The fresh 0.1Pt@S-1 catalyst has almost metallic Pt^0 NPs because the intensity of the white line in its XANES spectrum is very close to that of a Pt foil (Figure 1b). The CNs in Pt–O and Pt–Pt are 0.4 ± 0.3 and 12.6 ± 1.8, respectively (Table S3). These results suggest that a few peripheral Pt atoms of one NP are connected to the support via Pt–O bonds. After catalyst treatment in H_2 at 500 °C, the CN values decreased to 0.2 ± 0.2 and 10.3 ± 1.8. According to the results of O_2-pulse experiments (Figure S6b), the fraction of metallic Pt^0 in the reduced catalyst is about 98%.

The introduction of Pt to 1Co@S-1 did not affect the structure of CoO_x species in the fresh catalyst, as the Co-related features in the XANES spectra of the corresponding mono and

https://doi.org/10.1021/acscatal.5c08288
ACS Catal. XXXX, XXX, XXX–XXX

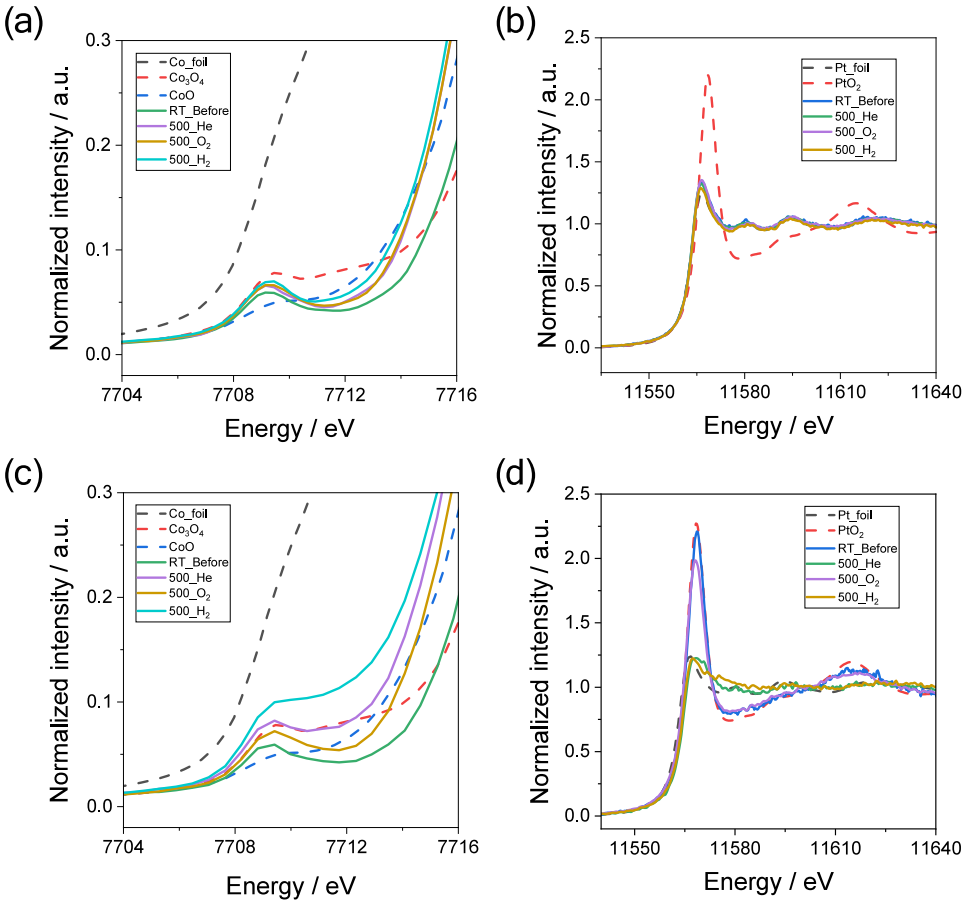

Figure 1. In situ XANES spectra of (a) 1Co@S-1, (b) 0.1Pt@S-1, and (c,d) 1Co-0.1Pt@S-1 at (a,c) Co k and (b,d) Pt-L_3 edges. Test conditions: heating in He to 500 °C followed by calcination in 20 vol % O_2/He and then reduction in 50 vol % H_2/He.

bimetallic catalysts are almost the same (Figure S7). It is, however, worth mentioning that the presence of Pt is decisive for the reducibility of CoO_x (Figure 1a,c). The fraction of metallic Co^0 in the reduced 1Co-0.1Pt@S-1 catalyst is about 16% and is obviously higher than 2% in the reduced 1Co@S-1 catalyst (Figure S6). The positive effect of Pt on the reduction degree of CoO_x can be explained by the ability of Pt to generate surface H species from H_2, which spill over to CoO_x and reduce them partially.

Based on the Pt-L_3-edge XANES spectra of the fresh 1Co-0.1Pt@S-1 catalyst and reference PtO_2, oxidized Pt nanoparticles (PtO_x) should be present in this catalyst (Figure 1d). A Pt–(O)–Co path with a distance of 2.72 Å was required to obtain a reasonable fit to the EXAFS spectrum of this catalyst (Table S5). This path, as well as the Pt–O path, could not be identified in the spectrum of the 1Co-0.1Pt@S-1 catalyst reduced in H_2 at 500 °C. Instead, a new PtCo path with a distance of about 0.15 Å shorter than 2.72 Å was identified. This path is characteristic of PtCo intermetallic compounds.[21] EXAFS wavelet-transform analysis using Pt foil and PtO_2 as references further confirms the formation of intermetallic PtCo in the reduced catalysts (Figure S8).

High-resolution transmission electron microscopy (HRTEM) could not identify Co or Pt nanoparticles on the surface of 1Co-0.1Pt@S-1 and 1Co@S-1 (Figures 2a and S9a–c). Ultrasmall clusters are present on the surface of 1Co-0.1Pt@S-1, as evidenced by AC-STEM (Figure 2b). The clusters consist of Co and Pt, according to energy-dispersive spectroscopy (EDS) line scans (Figure 2c). The atomic ratio of Pt:Co in these clusters should be 1:3 (Figure S1). EDS mapping further confirmed the high dispersion of Co and Pt (Figures 2d–i and S9d–g). Despite the low Pt loading in 0.1Pt@S-1, Pt nanoparticles could be observed on the surface of this catalyst (Figure S10). Therefore, Co should favor the dispersion of Pt in the 1Co-0.1Pt@S-1 catalyst.

In summary, the kind of supported species in the monometallic (Pt- or Co-containing) and bimetallic catalysts depends on the reaction atmosphere. Sub-nanometer CoO_x and PtO_x species are individually present on the surface of all catalysts treated in O_2. The CoO_x clusters in the 1Co@S-1 catalyst are only slightly reduced to Co^0 after reductive treatment in H_2 at 500 °C, while PtO_x in the 0.1Pt@S-1 catalyst is nearly to completely converted into Pt^0. In comparison with the reduced 1Co@S-1 catalyst, the reduction degree of CoO_x in the 1Co-0.1Pt@S-1 catalyst is significantly higher due to the positive effect of Pt. Consequently, this catalyst has PtCo intermetallic compound species in addition to CoO_x. The below section aims to provide insights into the kind of active species involved in the PDH reaction.

Intrinsic Catalyst Activity and Active Species. To compare the catalysts in terms of the rate of propene formation, we first carried out tests under differential reactor operation

https://doi.org/10.1021/acscatal.5c08288
ACS Catal. XXXX, XXX, XXX–XXX

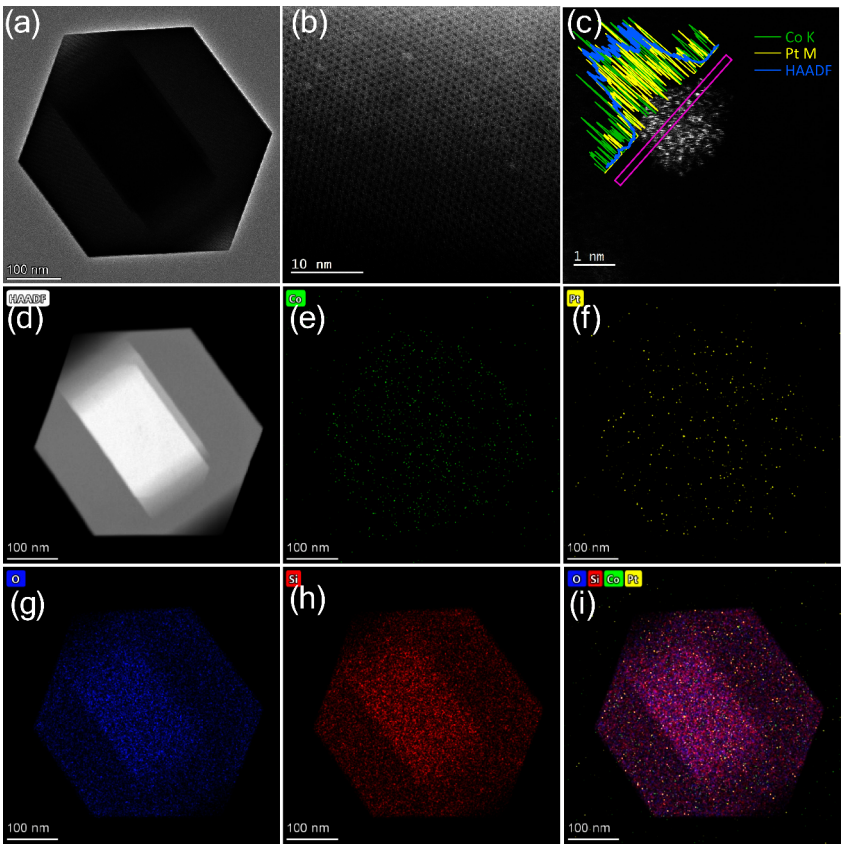

Figure 2. (a) HRTEM, (b) AC-STEM, and (c) AC-STEM images with an EDS line profile, as well as (d–i) HAADF-STEM images with EDS mapping of 1Co-0.1Pt@S-1.

conditions, i.e., the conversion of propane was below 10% of the equilibrium conversion. The catalysts were initially reduced in H_2 at 500 °C before starting the reaction at the same temperature to generate Pt^0, slightly reduced CoO_x or PtCo intermetallic compounds. The weight hourly space velocity of propane (WHSV(C_3H_8)) was varied between 38 and 378 h^{-1}. The rate obtained over all bimetallic Co-Pt@S-1 catalysts is higher than the rate over their monometallic counterparts (Figures 3a and S11). It reached 17.1 mmol·g^{-1}·min^{-1} with increasing Pt loading from 0.01 to 0.1 wt% at a fixed Co loading. In contrast to the reduced catalysts, the oxidized catalysts were less active (Figure S12). Thus, we put forward that the active species must be formed during reductive treatment of the catalysts in H_2 and/or in situ under the reaction conditions.

The rate of propene formation over reduced catalysts increases with increasing Co content from 0.25 to 1 wt% at a fixed Pt loading of 0.1 wt% (Figure S13). The highest synergistic effect between Pt and Co was determined for the 1Co-0.1Pt@S-1 catalyst. Its activity is 11 times higher than the sum of the propene formation rates determined over the 1Co@S-1 and 0.1Pt@S-1 catalysts. The reduction degree of CoO_x is less relevant to the catalyst activity because 1Co@S-1 reduced at 600 °C but tested in PDH at 500 °C showed almost the same activity as its counterpart reduced at 500 °C (Figure S14). The different activity of the monometallic and bimetallic catalysts should be related to the different kinds of active species/sites. The apparent activation energy (E_a) of propene formation over 1Co-0.1Pt@S-1 was determined to be 48 kJ·mol^{-1}. This value is meaningly lower than 105 and 91 kJ·mol^{-1} determined for 1Co@S-1 and 0.1Pt@S-1, respectively (Figure 3b).

Using catalytic data determined at different WHSV but at a constant temperature of 500 °C, we prepared selectivity–conversion relationships for propene, C_1–C_2 hydrocarbons, and coke formed in the PDH reaction over 1Co-0.1Pt@S-1, 0.1Pt@S-1, and 1Co@S-1. For all catalysts, the selectivity to propene decreases with increasing propane conversion (Figure 3c). An opposite trend was found for the selectivity to cracking products and coke (Figure 3d,e). Such results indicate that propene formed directly from propane is further converted into coke and cracking products. As the selectivity to C_1–C_2 hydrocarbons and coke extrapolated to zero propane conversion is not zero, these products should also be formed from propane. The contribution of this pathway decreases in the order 1Co@S-1 > 0.1Pt@S-1 > 1Co-0.1Pt@S-1. Moreover, the slope of the selectivity–conversion relationship for coke decreases in the same order, suggesting that the kind of active species affects this undesired pathway. Based on these results, the selectivity to propene is determined by the kinetics of primary and secondary pathways in the course of the PDH reaction (Figure 3f). Regardless of the propane conversion degree, the highest propene selectivity was achieved over 1Co-0.1Pt@S-1, followed by 0.1Pt@S-1 and 1Co@S-1. This is due to the lower ability of PtCo intermetallic compounds to convert both propane and propene to C_1–C_2 hydrocarbons and coke.

Based on the XAS and TEM data discussed above, as well as the catalytic data in Figure 3a, we can conclude that metallic

https://doi.org/10.1021/acscatal.5c08288
ACS Catal. XXXX, XXX, XXX–XXX

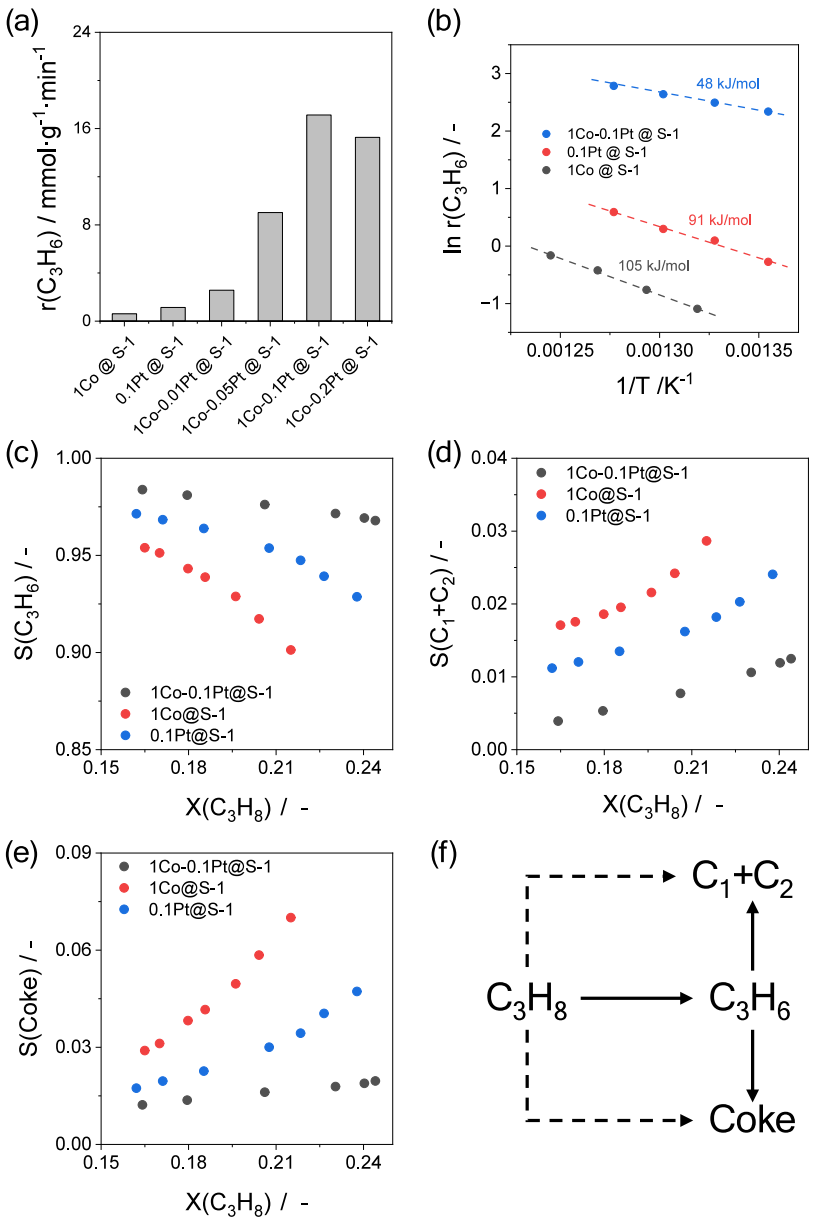

Figure 3. (a) Rate of propene formation ($r(C_3H_6)$) at 500 °C over the prepared catalysts. Reaction conditions for (a) T = 500 °C, C_3H_8:N_2 = 2:3, WHSV(C_3H_8) = 38–378 h^{-1}. (b) Arrhenius plots of the propene formation rate over 1Co-0.1Pt@S-1, 0.1Pt@S-1, and 1Co@S-1, as well as the respective apparent activation energy (E_a). All catalysts were reduced at 500 °C for 30 min in a flow of H_2/N_2 before the test. The selectivity–conversion relationships for (c) propene, (d) C_1–C_2 hydrocarbons, and (e) coke formed over 1Co@S-1, 0.1Pt@S-1, and 1Co-0.1Pt@S-1. (f) Proposed reaction pathways in the PDH reaction. Reaction conditions: T = 500 °C, C_3H_8:N_2 = 2:3, WHSV(C_3H_8) = 2.4–28.8 h^{-1}.

Pt^0, CoO_x, and metallic Co^0 show low PDH activity and propene selectivity. PtO_x can also be excluded as an active species because it does not exist under reaction conditions. Therefore, the PtCo intermetallic compound formed in situ should be responsible for the unexpectedly high activity of the 1Co-0.1Pt@S-1 catalyst.

Reaction Mechanism. To rationalize the difference in the PDH activity of metallic Pt^0, CoO_x, and PtCo, C_3H_8 pulse experiments were performed at 500 °C in a temporal analysis of products reactor.[38] The transient responses of C_3H_8, C_3H_6, H_2, and Ar are shown in Figures 4a and S15. Since C_3H_6 and H_2 are the products of C_3H_8 dehydrogenation, their responses appear after that of C_3H_8. Although the H_2 and C_3H_6 responses have very similar times of their maxima (t_{max}), the formation of H_2 must be decoupled from the formation of C_3H_6 and proceed at a lower rate because the diffusion coefficient of H_2 is about 4.6 times higher than that of C_3H_6, which is the reason for an earlier appearance of H_2 at the reactor outlet. For illustrative purposes, we converted the experimental time of the H_2 and C_3H_6 responses into a dimensionless time according to ref 39. The dimensionless time is defined as $t{\cdot}D_i/L^2$, where t is the experimental time, D_i is the effective diffusion coefficient of each component, and L is the reactor length. Such a transformation is useful for comparing the relative position of the responses of compounds with large differences in molecular mass (Figures 4b and S16). As expected, the maximum of the

https://doi.org/10.1021/acscatal.5c08288
ACS Catal. XXXX, XXX, XXX–XXX

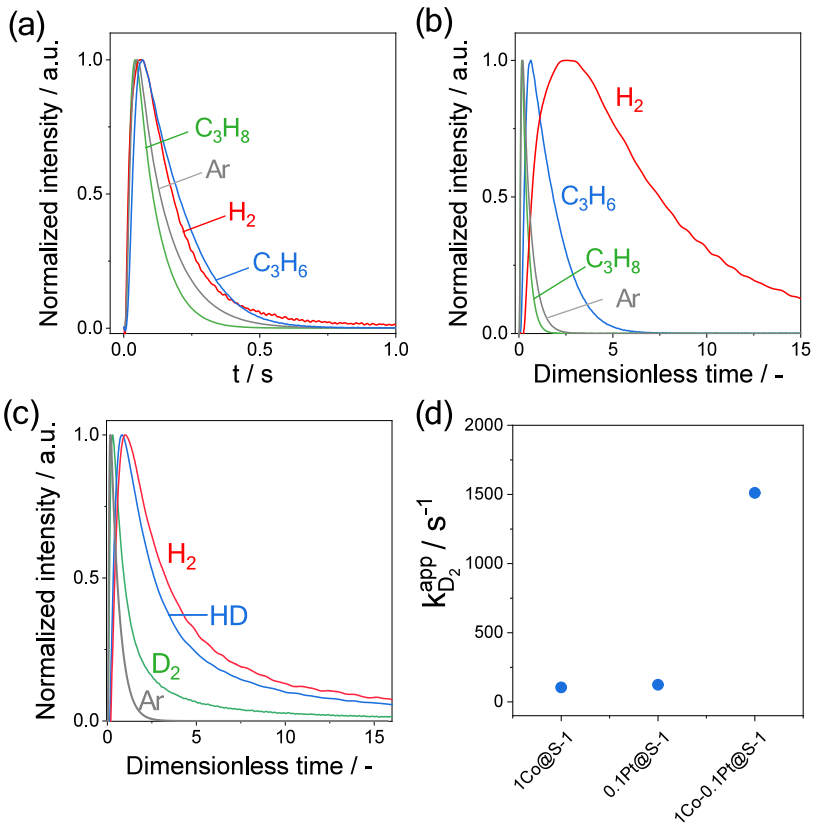

Figure 4. Normalized responses of C_3H_8, C_3H_6, H_2, and Ar after pulsing of a C_3H_8:Ar = 1:1 mixture over 1Co-0.1Pt@S-1 at 500 °C are shown in terms of (a) experimental time and (b) dimensionless time. (c) Normalized responses of D_2, HD, H_2, and Ar after pulsing of a D_2:Ar = 1:1 mixture over 1Co-0.1Pt@S-1 at 500 °C. The experimental time was transformed into dimensionless time according to ref 39. (d) Apparent rate constant of D_2 consumption over 1Co@S-1, 0.1Pt@S-1, and 1Co-0.1Pt@S-1 determined from pulse D_2:Ar = 1:1 tests at 500 °C according to ref 41.

normalized response of H_2 is significantly larger than that of the C_3H_6 response. Moreover, the experimental (not dimensionless) ratio of $t_{max}(H_2)/t_{max}(C_3H_6)$ should be about 0.86, which is higher than 0.5 for the case if H_2 and C_3H_6 were formed simultaneously.[40] Thus, the formation of H_2 should be the rate-limiting step in the PDH reaction. This assumption was indirectly supported by a temperature-programmed surface reaction experiment with C_3H_8. We found that the temperature at which H_2 starts to be formed is higher than that of C_3H_6 (Figure S17).

Based on the above discussion, the catalyst ability to activate H_2 can be one of the key factors determining the rate of propene production. This assumption was validated by H–D exchange tests with 1Co@S-1, 0.1Pt@S-1, and 1Co-0.1Pt@S-1. HD and H_2 were detected when a mixture of D_2/Ar = 1:1 was pulsed over these catalysts at 500 °C (Figures 4c and S18). Their formation indicates that (i) the catalysts can break the D–D bond in D_2, (ii) the catalysts have active OH groups, and (iii) the D atoms formed on CoO_x, Pt, and CoPt can react with these groups to form initially HD (its response appears directly after D_2). This reaction product participates in a consecutive exchange with OH groups, finally yielding H_2. Applying the thin-zone TAP reactor model,[41] an apparent rate constant ($k_{D_2}^{app}$) of D_2 activation was estimated (eq 2). 1Co@S-1 and 0.1Pt@S-1 have the lowest $k_{D_2}^{app}$ values (Figure 4d). The $k_{D_2}^{app}$ value of the 1Co-0.1Pt@S-1 catalyst is approximately 12 times higher compared to the corresponding monometallic counterparts.

Deeper molecular-level insights were derived using density functional theory (DFT) calculations. Based on the TEM and EXAFS fitting results, we created the Pt_4Co_{12}@S-1 model representing the structure of the active species in the reduced 1Co-0.1Pt@S-1 catalyst. The Gibbs free energy profile for propane dehydrogenation at 500 °C was then evaluated for this model system (Figure 5a,b). Adsorption of propane is thermodynamically unfavorable ($\Delta G = 0.64$ eV), indicating weak interaction between propane and the cluster under reaction conditions. The first C–H bond cleavage proceeds with an activation barrier of 0.39 eV, forming a surface propyl species together with an adsorbed hydrogen atom. The subsequent C–H cleavage occurs with an activation barrier of approximately 0.60 eV and leads to the formation of propylene and two hydrogen atoms bound to the cluster. Desorption of propylene is thermodynamically favorable, leaving hydrogen atoms on the cluster surface. Before recombination, one hydrogen species migrates to the same Pt atom where another hydrogen atom is located, with a small activation barrier of 0.11 eV. Thereafter, recombination of the two hydrogen atoms occurs, leading to the formation of adsorbed H_2, which is energetically unfavorable. Both the migration and recombination steps are needed for the recovery of the active site, with an overall energy span of 0.66 eV. Thus, the regeneration of the active sites should limit the overall kinetics of the PDH reaction. The reverse process (H_2 dissociation on the cluster surface) is barrierless, suggesting that hydrogen tends to dissociate upon

https://doi.org/10.1021/acscatal.5c08288
ACS Catal. XXXX, XXX, XXX–XXX

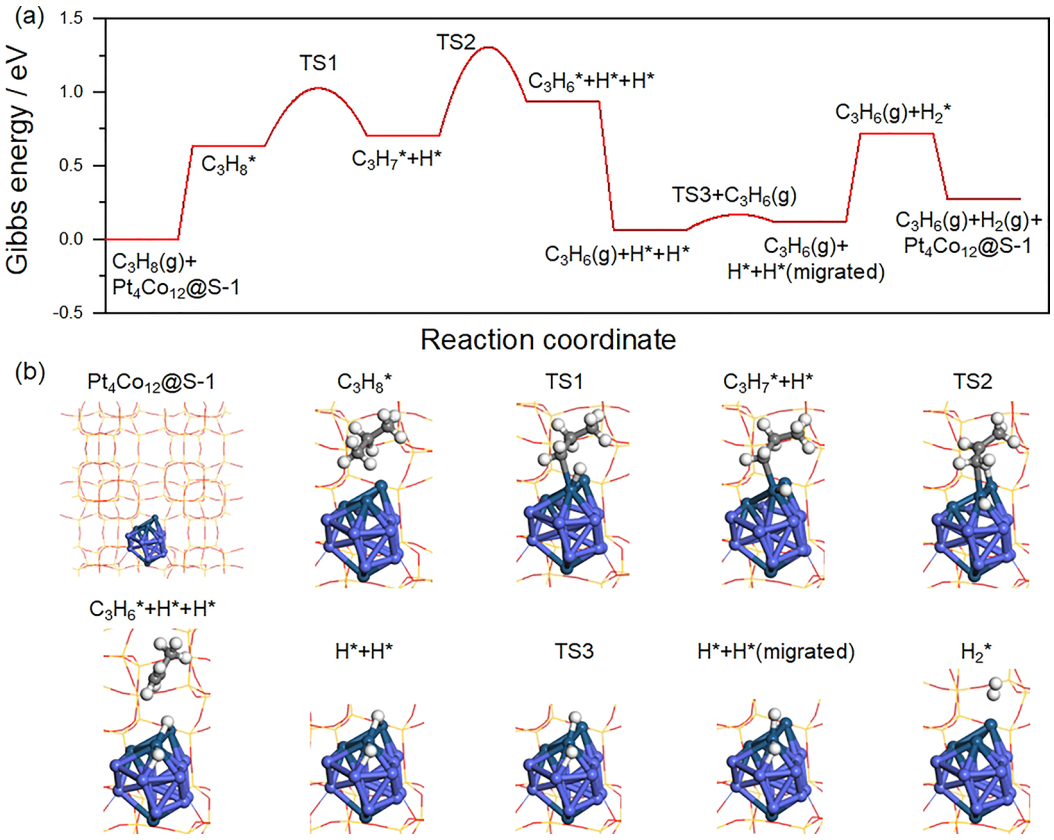

Figure 5. (a) Gibbs free energy profiles calculated for propane dehydrogenation at 500 °C and ambient pressure over the Pt_4Co_{12}@S-1 catalyst. (b) Optimized structures of intermediates and transition states obtained along the reaction pathway. Color scheme: Pt—blue, Co—purple, C—gray, H—white; the lines represent the framework of the MFI zeolite. Coordinates of the illustrated structures, as well as the calculated frequencies of the adsorbates, are provided in the Supporting Information under the sections "Optimized Coordinates" and "Frequencies," respectively.

adsorption. This behavior is in good agreement with previous reports on hydrogen activation on platinum-based catalysts.[42]

Industrial Relevance. To demonstrate the industrial potential of the 1Co-0.1Pt@S-1 catalyst, its PDH performance was directly compared with that of an analog of a commercial Pt–Sn/Al_2O_3 catalyst tested at 500 °C in parallel using a feed with 40 vol % C_3H_8 at WHSV(C_3H_8) of 31.4 h^{-1} (Figure S19). The initial propane conversion of 23%, about 91% of the equilibrium conversion ($X(C_3H_8)_{eq}$), was achieved over our catalyst, while the reference reached only 12% conversion. The latter catalyst also lost much of its initial conversion with increasing time on stream, in contrast to the stable performance of the 1Co-0.1Pt@S-1 catalyst, although the Pt loading in the developed catalyst is only 20% of its reference counterpart. The long-term stability of the 1Co-0.1Pt@S-1 catalyst was also validated under harsher reaction conditions using a feed with 90 vol % C_3H_8 at WHSV(C_3H_8) of 35 h^{-1} (Figure 6a). The catalyst slightly deactivated during 110 h on propane due to reaction-induced restructuring of active species. (Figure S20). The initial propane conversion was about 90% of $X(C_3H_8)_{eq}$. Noticeably, the outlet propene concentration in this test was above 14 vol %, which is similar to that of the Oleflex and Uhde processes operating at higher temperatures (Figure S21). As propene is the key gas-phase precursor of coke, the apparent deactivation rate constant (k_d) of 4×10^{-4} h^{-1} at such a high propene concentration is worth mentioning and proves the unanticipated resistance of this catalyst to coke formation (Figure S22). Moreover, the low k_d value was obtained at a high integral propene formation rate of 132 $mol_{C3H6} \cdot g_{Pt}^{-1} \cdot h^{-1}$. In this respect, the developed catalyst outperformed many Pt-based catalysts from a recent review[3] (Figure 6b).

We also benchmarked the 1Co-0.1Pt@S-1 catalyst against state-of-the-art Pt-based catalysts in terms of space–time yield of propene formation related to (i) overall catalyst amount ($STY(C_3H_6)$) or (ii) Pt loading ($STY(C_3H_6)_{Pt}$). To ensure a proper comparison of the catalysts tested in different studies, we plotted the $STY(C_3H_6)$ and $STY(C_3H_6)_{Pt}$ values versus the ratio of the experimentally determined propane conversion to the corresponding equilibrium propane conversion ($X(C_3H_8)_{exp}/X(C_3H_8)_{eq}$) in Figures 6c and S23, respectively. The present $STY(C_3H_6)$ values achieved at 500 and 550 °C were 5.6 and 25.7 $kg \cdot kg_{cat}^{-1} \cdot h^{-1}$at about 90 and 64% equilibrium propane conversion, respectively (Figures 6c and S24). These values are higher than those of most reported Pt-containing catalysts tested at the same or higher temperatures (Figure 6c). Considering the low Pt content, the 1Co-0.1Pt@S-1 catalyst outperforms all previously reported catalysts in terms of $STY(C_3H_6)_{Pt}$, as seen in Figure S23.

A series of six PDH/regeneration cycles were carried out to test catalyst durability (Figure S25). Although no deactivation of the catalyst was observed within each PDH cycle lasting for 1 h, the catalyst showed lower conversion in subsequent PDH cycles after oxidative treatment. This decrease in conversion

https://doi.org/10.1021/acscatal.5c08288
ACS Catal. XXXX, XXX, XXX–XXX

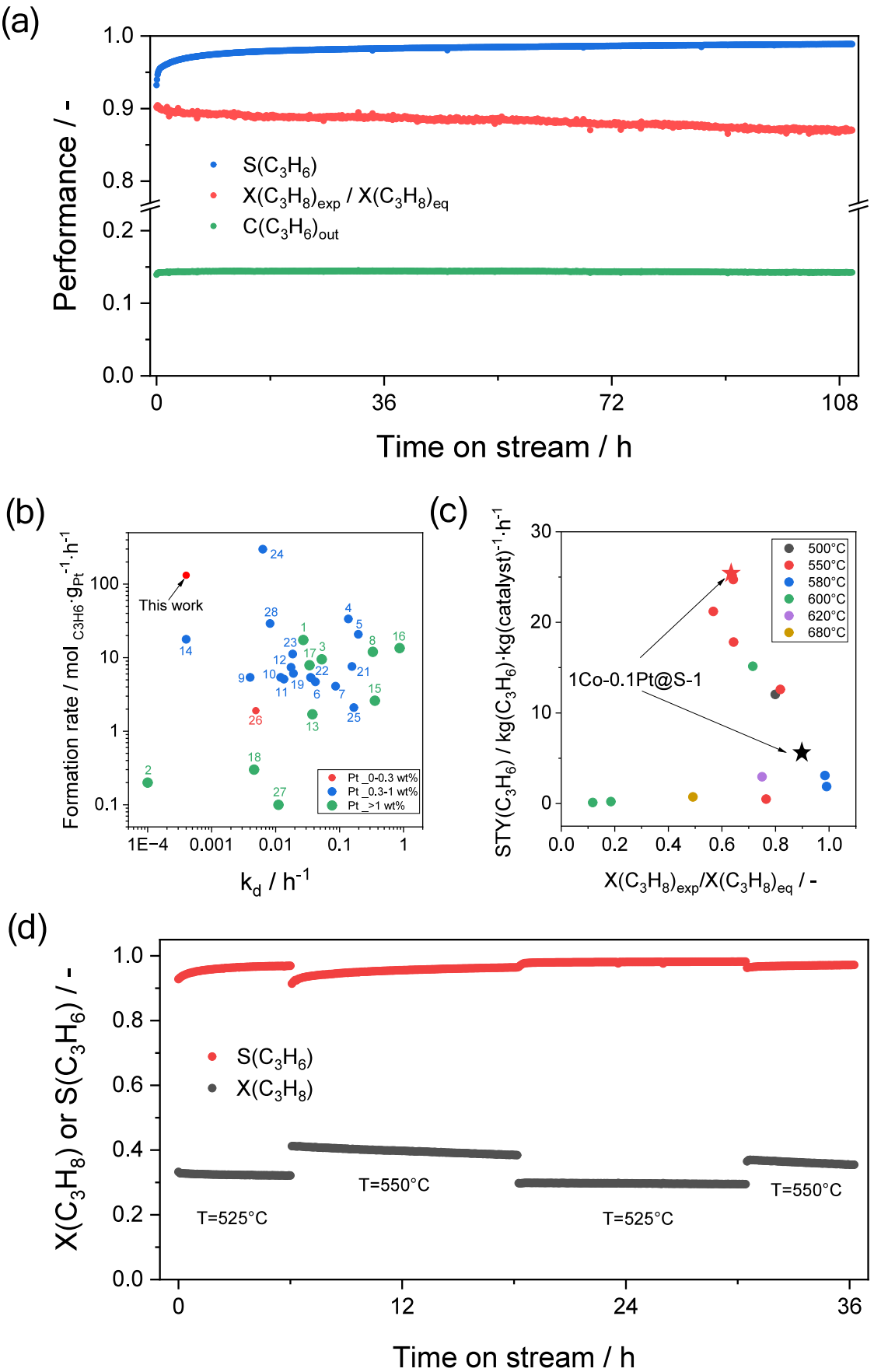

Figure 6. (a) On-stream profiles of $X(C_3H_8)_{exp}/X(C_3H_8)_{eq}$, outlet propene concentration ($C(C_3H_6)_{out}$), and propene selectivity over 1Co-0.1Pt@S-1 in a 110 h PDH test at 500 °C, using a feed with 90 vol % C_3H_8 at WHSV(C_3H_8) of 35 h^{-1}. (b) Rate of propene formation versus

https://doi.org/10.1021/acscatal.5c08288
ACS Catal. XXXX, XXX, XXX−XXX

Figure 6. continued

deactivation rate constant (k_d) determined for 1Co-0.1Pt@S-1 and different Pt-based catalysts (Table S6). (c) STY(C_3H_6) determined over 1Co-0.1Pt@S-1 and literature reported Pt-based catalysts (Table S7) versus $X(C_3H_8)_{exp}/X(C_3H_8)_{eq}$. Reaction conditions: T = 500 or 550 °C, C_3H_8:N_2 = 9:1 or C_3H_8:N_2 = 4:6, WHSV(C_3H_8) = 35.4 or 94.3 h^{-1}. (d) Time-on-stream profiles of propane conversion and propene selectivity over 1Co-0.1Pt@S-1. Reaction conditions for (d): T = 525–550 °C, C_3H_8:N_2 = 2:3, WHSV(C_3H_8) = 15.7 h^{-1}.

became less pronounced from cycle to cycle. To get an insight into the origin of the catalyst deactivation, the spent catalyst after six cycles was characterized by HRTEM. Agglomerated Pt particles were identified on its surface (Figure S26).

To further demonstrate the industrial relevance of the developed catalyst, we performed an additional stability test at 525 and 550 °C using a reaction feed with 40 vol% C_3H_8 at WHSV(C_3H_8) of 15.7 h^{-1} (Figure 6d). The conversion of propane was above 30% (above 90% of $X(C_3H_8)_{eq}$) and 35% (above 84% of $X(C_3H_8)_{eq}$) within 36 h on propane stream at 525 and 550 °C, respectively. The corresponding propene selectivity values were above 95 and 93%. The major challenges hindering industrial application of PtCo/silicalite-1 materials are to improve their durability and to provide an economically feasible preparation method with hydrothermal crystallization of silicalite-1.

■ CONCLUSIONS

In summary, the results obtained in this study show that the promotion of Co/silicalite-1 with minute amounts (up to 1000 ppm) of Pt results in highly active, stable, and durable PDH catalysts. The most active 1Co-0.1Pt@S-1 catalyst outperforms state-of-the-art Pt-based catalysts including an analog of a commercial Pt–Sn/Al_2O_3 catalyst tested in parallel, in terms of the space–time yield of propene formation under close-to-equilibrium conditions using an industrially relevant reaction feed. Complementary characterization analysis revealed that sub-nanosized PtCo intermetallic compounds formed in situ within the support act as active species. They show a lower ability to undergo consecutive transformations of propene to coke and C_1–C_2 hydrocarbons in comparison to monometallic Pt or CoO_x species. This is advantageous for achieving propene selectivity of over 95% at propane conversion close to equilibrium.

■ ASSOCIATED CONTENT

Supporting Information

The Supporting Information is available free of charge at https://pubs.acs.org/doi/10.1021/acscatal.5c08288.

Element composition, XRD patterns, UV–vis spectra, Co 2p XP spectra, XANES spectra, HRTEM and HAADF-STEM images, coordinates of atoms in the optimized structures, and frequencies of the adsorbates for these structures (PDF)

■ AUTHOR INFORMATION

Corresponding Authors

Tatiana Otroshchenko – *Leibniz Institut für Katalyse e.V., Albert-Einstein-Str. 29a, Rostock 18059, Germany;* orcid.org/0000-0003-0157-3479; Email: tatiana.otroshchenko@catalysis.de

Dan Zhao – *Leibniz Institut für Katalyse e.V., Albert-Einstein-Str. 29a, Rostock 18059, Germany; National Engineering Research Centre of Lower-Carbon Catalysis Technology, Dalian National Laboratory for Clean Energy, Dalian Institute of Chemical Physics, Chinese Academy of Sciences, Dalian 116023, P. R. China;* Email: zhaodan92@dicp.ac.cn

Evgenii V. Kondratenko – *Leibniz Institut für Katalyse e.V., Albert-Einstein-Str. 29a, Rostock 18059, Germany;* orcid.org/0000-0003-0431-6937; Email: evgenii.kondratenko@catalysis.de

Authors

Qiyang Zhang – *Leibniz Institut für Katalyse e.V., Albert-Einstein-Str. 29a, Rostock 18059, Germany*

Mingbin Gao – *State Key Laboratory of Physical Chemistry of Solid Surfaces, College of Chemistry and Chemical Engineering, Xiamen University, Xiamen 361005, China;* orcid.org/0000-0002-7143-2658

Vita A. Kondratenko – *Leibniz Institut für Katalyse e.V., Albert-Einstein-Str. 29a, Rostock 18059, Germany*

Xiangnong Ding – *Leibniz Institut für Katalyse e.V., Albert-Einstein-Str. 29a, Rostock 18059, Germany*

Dmitry E. Doronkin – *National Institute for Chemical Technology and Polymer Chemistry, and Institute of Catalysis Research and Technology, Karlsruhe Institute of Technology, Kaiserstr. 12, Karlsruhe D-76131, Germany;* orcid.org/0000-0003-3930-3204

Dongxu Wang – *Max Planck Institute of Microstructure Physics, Weinberg 2, Halle 06120, Germany*

Dong Li – *#Institute of Catalysis for Energy and Environment, College of Chemistry and Chemical Engineering, Shenyang Normal University, 253# Huanghe North Street, Huanggu District, Shenyang 110034, China*

Complete contact information is available at: https://pubs.acs.org/doi/10.1021/acscatal.5c08288

Author Contributions

The manuscript was written through contributions of all authors. All authors have given approval to the final version of the manuscript.

Notes

The authors declare no competing financial interest.

■ ACKNOWLEDGMENTS

Financial support by the State of Mecklenburg-Vorpommern is gratefully acknowledged. We acknowledge DESY (Hamburg, Germany), a member of the Helmholtz Association HGF, for the prevision of experimental facilities. Parts of this research were carried out at PETRA III, and we would like to thank Dr. Edmund Welter for assistance in using beamline P65. Beamtime was granted for the proposal I-20230812 and I-20240852.

■ REFERENCES

(1) Otroshchenko, T.; Jiang, G.; Kondratenko, V. A.; Rodemerck, U.; Kondratenko, E. V. Current status and perspectives in oxidative, non-

oxidative and CO_2-mediated dehydrogenation of propane and isobutane over metal oxide catalysts. *Chem. Soc. Rev.* **2021**, *50* (1), 473–527.
(2) Dai, Y.; Gao, X.; Wang, Q.; Wan, X.; Zhou, C.; Yang, Y. Recent progress in heterogeneous metal and metal oxide catalysts for direct dehydrogenation of ethane and propane. *Chem. Soc. Rev.* **2021**, *50* (9), 5590–5630.
(3) Chen, S.; Chang, X.; Sun, G.; Zhang, T.; Xu, Y.; Wang, Y.; Pei, C.; Gong, J. Propane dehydrogenation: catalyst development, new chemistry, and emerging technologies. *Chem. Soc. Rev.* **2021**, *50* (5), 3315–3354.
(4) Gholami, Z.; Gholami, F.; Tišler, Z.; Vakili, M. A review on the production of light olefins using steam cracking of hydrocarbons. *Energies* **2021**, *14* (23), 8190.
(5) Tian, P.; Wei, Y.; Ye, M.; Liu, Z. Methanol to olefins (MTO): from fundamentals to commercialization. *ACS Catal.* **2015**, *5* (3), 1922–1938.
(6) Zhang, Q.; Xiao, T.; Liu, C.; Otroshchenko, T.; Kondratenko, E. V. Performance Descriptors for Catalysts Based on Molybdenum, Tungsten, or Rhenium Oxides for Metathesis of Ethylene with 2-Butenes to Propene. *Angew. Chem., Int. Ed.* **2023**, *62* (40), No. e202308872.
(7) Zhai, P.; Li, Y.; Wang, M.; Liu, J.; Cao, Z.; Zhang, J.; Xu, Y.; Liu, X.; Li, Y.-W.; Zhu, Q. Development of direct conversion of syngas to unsaturated hydrocarbons based on Fischer-Tropsch route. *Chem* **2021**, *7* (11), 3027–3051.
(8) Zhao, D.; Tian, X.; Doronkin, D. E.; Han, S.; Kondratenko, V. A.; Grunwaldt, J.-D.; Perechodjuk, A.; Vuong, T. H.; Rabeah, J.; Eckelt, R. In situ formation of ZnO_x species for efficient propane dehydrogenation. *Nature* **2021**, *599* (7884), 234–238.
(9) Sattler, J. J.; Ruiz-Martinez, J.; Santillan-Jimenez, E.; Weckhuysen, B. M. Catalytic dehydrogenation of light alkanes on metals and metal oxides. *Chem. Rev.* **2014**, *114* (20), 10613–10653.
(10) Motagamwala, A. H.; Almallahi, R.; Wortman, J.; Igenegbai, V. O.; Linic, S. Stable and selective catalysts for propane dehydrogenation operating at thermodynamic limit. *Science* **2021**, *373* (6551), 217–222.
(11) Ryoo, R.; Kim, J.; Jo, C.; Han, S. W.; Kim, J.-C.; Park, H.; Han, J.; Shin, H. S.; Shin, J. W. Rare-earth–platinum alloy nanoparticles in mesoporous zeolite for catalysis. *Nature* **2020**, *585* (7824), 221–224.
(12) Xu, Z.; Yue, Y.; Bao, X.; Xie, Z.; Zhu, H. Propane dehydrogenation over Pt clusters localized at the Sn single-site in zeolite framework. *ACS Catal.* **2019**, *10* (1), 818–828.
(13) Shi, L.; Deng, G. M.; Li, W. C.; Miao, S.; Wang, Q. N.; Zhang, W. P.; Lu, A. H. Al_2O_3 nanosheets rich in pentacoordinate Al^{3+} ions stabilize Pt-Sn clusters for propane dehydrogenation. *Angew. Chem., Int. Ed.* **2015**, *54* (47), 13994–13998.
(14) Xu, Z.; Gao, M.; Wei, Y.; Yue, Y.; Bai, Z.; Yuan, P.; Fornasiero, P.; Basset, J.-M.; Mei, B.; Liu, Z. Pt migration–lockup in zeolite for stable propane dehydrogenation catalyst. *Nature* **2025**, *643* (8072), 691–698.
(15) Hong, H.; Xu, Z.; Mei, B.; Hu, W.; Fornasiero, P.; Wang, C.; Wang, T.; Yue, Y.; Li, T.; Yang, C. A self-regenerating Pt/Ge-MFI zeolite for propane dehydrogenation with high endurance. *Science* **2025**, *388* (6746), 497–502.
(16) Nakaya, Y.; Xing, F.; Ham, H.; Shimizu, K. i.; Furukawa, S. Doubly decorated platinum–gallium intermetallics as stable catalysts for propane dehydrogenation. *Angew. Chem., Int. Ed.* **2021**, *60* (36), 19715–19719.
(17) Chen, S.; Zhao, Z.-J.; Mu, R.; Chang, X.; Luo, J.; Purdy, S. C.; Kropf, A. J.; Sun, G.; Pei, C.; Miller, J. T. Propane dehydrogenation on single-site [PtZn4] intermetallic catalysts. *Chem* **2021**, *7* (2), 387–405.
(18) Qian, R.; Luo, S.-z.; Jing, F.; Fang, W. Carbon nanotubes confined PtIn alloy as a highly stable catalyst for propane dehydrogenation. *Ind. Eng. Chem. Res.* **2022**, *61* (47), 17264–17274.
(19) Liu, X.; Wang, X.; Zhen, S.; Sun, G.; Pei, C.; Zhao, Z.-J.; Gong, J. Support stabilized PtCu single-atom alloys for propane dehydrogenation. *Chem. Sci.* **2022**, *13* (33), 9537–9543.
(20) Ma, Z.; Wu, Z.; Miller, J. T. Effect of Cu content on the bimetallic Pt–Cu catalysts for propane dehydrogenation. *Catal. Struct. React.* **2017**, *3* (1-2), 43–53.
(21) Cesar, L. G.; Yang, C.; Lu, Z.; Ren, Y.; Zhang, G.; Miller, J. T. Identification of a Pt_3Co surface intermetallic alloy in Pt–Co propane dehydrogenation catalysts. *ACS Catal.* **2019**, *9* (6), 5231–5244.
(22) Zhang, Q.; Li, Y.; Otroshchenko, T.; Kondratenko, V. A.; Wu, K.; Fedorova, E. A.; Doronkin, D. E.; Bartling, S.; Lund, H.; Jiang, G. The enhancing effect of Co^{2+} on propane non-oxidative dehydrogenation over supported Co/ZrO_2 catalysts. *J. Catal.* **2024**, *432*, No. 115440.
(23) Hu, Z.-P.; Qin, G.; Han, J.; Zhang, W.; Wang, N.; Zheng, Y.; Jiang, Q.; Ji, T.; Yuan, Z.-Y.; Xiao, J. Atomic insight into the local structure and microenvironment of isolated Co-motifs in MFI zeolite frameworks for propane dehydrogenation. *J. Am. Chem. Soc.* **2022**, *144* (27), 12127–12137.
(24) Xu, D.; Li, Q. Y.; Su, Q. X.; Xia, S. Y.; Xu, Y. S.; Leng, B. L.; Lin, X.; Fan, L. Y.; Chen, J. S.; Li, X. H. Boosting Propane Dehydrogenation to Propylene via Electron Hole-Hydrogen Coupling on Cobalt Metal Surface. *Angew. Chem., Int. Ed.* **2025**, *64* (7), No. e202419816.
(25) Iglesias-Juez, A.; Beale, A. M.; Maaijen, K.; Weng, T. C.; Glatzel, P.; Weckhuysen, B. M. A combined in situ time-resolved UV–Vis, Raman and high-energy resolution X-ray absorption spectroscopy study on the deactivation behavior of Pt and PtSn propane dehydrogenation catalysts under industrial reaction conditions. *J. Catal.* **2010**, *276* (2), 268–279.
(26) Rochlitz, L.; Searles, K.; Alfke, J.; Zemlyanov, D.; Safonova, O. V.; Copéret, C. Silica-supported, narrowly distributed, subnanometric Pt–Zn particles from single sites with high propane dehydrogenation performance. *Chem. Sci.* **2020**, *11* (6), 1549–1555.
(27) Wu, Z.; Bukowski, B. C.; Li, Z.; Milligan, C.; Zhou, L.; Ma, T.; Wu, Y.; Ren, Y.; Ribeiro, F. H.; Delgass, W. N. Changes in catalytic and adsorptive properties of 2 nm Pt3Mn nanoparticles by subsurface atoms. *J. Am. Chem. Soc.* **2018**, *140* (44), 14870–14877.
(28) Deng, L.; Miura, H.; Shishido, T.; Wang, Z.; Hosokawa, S.; Teramura, K.; Tanaka, T. Elucidating strong metal-support interactions in $Pt–Sn/SiO_2$ catalyst and its consequences for dehydrogenation of lower alkanes. *J. Catal.* **2018**, *365*, 277–291.
(29) Sun, P.; Siddiqi, G.; Vining, W. C.; Chi, M.; Bell, A. T. Novel Pt/Mg (In)(Al) O catalysts for ethane and propane dehydrogenation. *J. Catal.* **2011**, *282* (1), 165–174.
(30) Siddiqi, G.; Sun, P.; Galvita, V.; Bell, A. T. Catalyst performance of novel Pt/Mg (Ga)(Al) O catalysts for alkane dehydrogenation. *J. Catal.* **2010**, *274* (2), 200–206.
(31) Grimme, S.; Antony, J.; Ehrlich, S.; Krieg, H. A consistent and accurate ab initio parametrization of density functional dispersion correction (DFT-D) for the 94 elements H-Pu. *J. Chem. Phys.* **2010**, *132* (15), No. 154104.
(32) Henkelman, G.; Uberuaga, B. P.; Jónsson, H. A climbing image nudged elastic band method for finding saddle points and minimum energy paths. *J. Chem. Phys.* **2000**, *113* (22), 9901–9904.
(33) Heyden, A.; Bell, A. T.; Keil, F. J. Efficient methods for finding transition states in chemical reactions: Comparison of improved dimer method and partitioned rational function optimization method. *J. Chem. Phys.* **2005**, *123* (22).
(34) Wang, V.; Xu, N.; Liu, J.-C.; Tang, G.; Geng, W.-T. VASPKIT: A user-friendly interface facilitating high-throughput computing and analysis using VASP code. *Comput. Phys. Commun.* **2021**, *267*, No. 108033.
(35) Wu, L.; Ren, Z.; He, Y.; Yang, M.; Yu, Y.; Liu, Y.; Tan, L.; Tang, Y. Atomically dispersed Co^{2+} sites incorporated into a silicalite-1 zeolite framework as a high-performance and coking-resistant catalyst for propane nonoxidative dehydrogenation to propylene. *ACS Appl. Mat. Interfaces* **2021**, *13* (41), 48934–48948.
(36) Yamamoto, T. Assignment of pre-edge peaks in K-edge x-ray absorption spectra of 3d transition metal compounds: Electric dipole or quadrupole?. *X-Ray Spectrom.: Int. J.* **2008**, *37* (6), 572–584.
(37) Hunault, M.; Vercamer, V.; Haverkort, M. W.; Arrio, M. A.; Brouder, C.; Calas, G.; Juhin, A. Tracking the signature of low symmetry environments in the XAS K pre-edge.. *J. Phys.: Conf. Ser.* **2016**, *712* (1), No. 012005.
(38) Otroshchenko, T.; Kondratenko, V. A.; Zanina, A.; Zhang, Q.; Kondratenko, E. V. Progress through Temporal Analysis of Products

https://doi.org/10.1021/acscatal.5c08288
ACS Catal. XXXX, XXX, XXX–XXX

and Steady-state Isotopic Transient Kinetic Analysis to Elucidate Oxidation, CO_2 Hydrogenation and Lower Olefins Production Reactions. *ChemCatChem* **2024**, *16* (16), No. e202400081.

(39) Gleaves, J. T.; Yablonskii, G. S.; Phanawadee, P.; Schuurman, Y. TAP-2: An interrogative kinetics approach. *Appl. Catal. A.* **1997**, *160* (1), 55–88.

(40) Wu, K.; Kondratenko, V. A.; Zhou, M.; Doronkin, D. E.; Bartling, S.; Zhang, Q.; Han, S.; Jia, X.; Liu, Q.; Xiong, D. The Role of Reducibility of $PtGaO_x$-Based Catalysts for Efficient and Durable Propane Dehydrogenation. *Angew. Chem., Int. Ed.* **2025**, *64* (31), No. e202506704.

(41) Gleaves, J. T.; Yablonsky, G.; Zheng, X.; Fushimi, R.; Mills, P. L. Temporal analysis of products (TAP)—recent advances in technology for kinetic analysis of multi-component catalysts. *J. Mol. Catal. A* **2010**, *315* (2), 108–134.

(42) Wu, Q.; Xiong, W.; Yang, G. H_2 Activation and Adsorbed H Species on Pt-Based Heterogeneous Catalysts: Fundamentals and Advances. *ChemCatChem* **2025**, *17* (18), No. e00902.

https://doi.org/10.1021/acscatal.5c08288
ACS Catal. XXXX, XXX, XXX–XXX